Supporting Information

Low electron affinity silicon/nanocrystalline diamond heterostructures for photon-enhanced thermionic emission

Raffaella Salerno[§,*], Veronica Valentini[∇], Eleonora Bolli[∇], Matteo Mastellone[∇], Valerio Serpente[∇], Alessio Mezzi[‖], Luca Tortora[⊥,$], Elisabetta Colantoni[£], Alessandro Bellucci[∇,*], Riccardo Polini[§], and Daniele M. Trucchi[∇]

§ Università di Roma "Tor Vergata", Dipartimento di Scienze e Tecnologie Chimiche, Via della Ricerca Scientifica 1, 00133 Roma, Italy.

∇Istituto di Struttura della Materia (ISM-CNR), Consiglio Nazionale delle Ricerche, DiaTHEMA Lab, Sede Secondaria di Montelibretti, Via Salaria km 29.300, 00015 Monterotondo Stazione, Roma, Italy.

‖Istituto per lo Studio dei Materiali Nanostrutturati (ISMN-CNR), Consiglio Nazionale delle Ricerche, Via Salaria km 29.300, 00015 Monterotondo Stazione, Roma, Italy.

⊥Università degli Studi RomaTre, Dipartimento di Scienze, via della Vasca Navale 84, 00146 Roma, Italy

$ Istituto Nazionale di Fisica Nucleare (INFN) sezione Roma Tre, via della Vasca Navale 84, 00146 Roma, Italy

£ Università degli Studi RomaTre, Dipartimento di Matematica e Fisica, via della Vasca Navale 84, 00146 Roma, Italy

Corresponding authors: alessandro.bellucci@ism.cnr.it; raffaella.salerno@ism.cnr.it.

Summary

This document is sub-divided into the following five sections:

1. Experimental details on material preparation and characterization
2. Scanning Electron Microscope (SEM) investigation
3. Additional details on the KPFM analysis
4. Time-of-Flight Secondary Ion Mass Spectrometry (TOF-SIMS) data
5. X-ray Photo-electron Spectroscopy (XPS) data and additional details on the UPS analysis
6. Experimental setup for the PETE measurements

1. Experimental details on material preparation and characterization

The five silicon-diamond 1 x 1 cm photocathodes used in this study were created through the deposition of nanocrystalline diamond films of different thicknesses on boron doped p-type (100) silicon substrates (270 ± 25 μm thickness, 1–5 mΩ·cm resistivity, surface roughness < 1 nm) provided by University Wafer Inc. The silicon wafers underwent a cleaning pretreatment and seeding process. The cleaning process consisted of a 10 minutes acetone ultrasonic bath, 10 minutes 2-propanol ultrasonic bath and 3 minutes HF:H_2O = 1:9 ultrasonic bath followed by rinsing with deionized water. The clean silicon wafer was seeded by immersion and sonication in a detonation nanodiamond (DND) suspension obtained mixing the Dimethyl sulfoxide Blueseeds suspension (Adámas Nanotechnology) with Methanol in a 1:3 ratio for 15 minutes. The silicon wafers were rinsed with methanol and dried with a compressed air flow.

Diamond film growth was accomplished with a customized ASTeX microwave plasma assisted CVD reactor set at 800 W microwave power, 27 Torr chamber pressure and 1% CH4 to H_2 percentage ratio. Deposition times of 8, 16, 32, 80 and 160 minutes produced ~ 40, 80, 180, 550 and 1040 nm thick diamond films. The diamond surfaces of the photocathodes subsequently underwent a 15-minute plasma treatment in an atmosphere of pure hydrogen to homogenize the hydrogenation of the diamond surfaces.

Titanium metal contacts were applied to the silicon side of the photocathodes via radiofrequency magnetron sputtering (Leybold LH Z400).

The surface morphology and diamond film thickness were determined with a field emission gun scanning electron microscope (FEG SEM, Zeiss LEO Supra 35). All the images were acquired using the secondary electron Inlens detector at 10 kV.

Raman measurements were carried out using a Horiba Scientific LabRam HR Evolution confocal spectrometer equipped with a 100mW Oxxius (wavelength of 532 nm) laser source and a computerized XY-table, an electron-multiplier CCD detector, and an Olympus U5RE2 microscope with a 100x objective (laser spot on the sample surface 0.7 μm) with a numerical aperture (NA) of 0.9, and a grating with 600 grooves/mm were used. All Raman spectra were recorded in backscattering geometry focalizing 10% of the laser sources power at the sample and ten spectra with an accumulation time of 10 s were averaged. Samples were measured before and after a hydrogenation treatment.

Kelvin Probe Force Microscopy (KPFM) analyses were performed using an an OmegaScope platform (HORIBA Ltd., Kyoto, Japan). The samples were sequentially mounted on special sample holder equipped with a metal clip to avoid possible potential electrostatic charge effects.

XPS and UPS measurements were performed by using an ESCALAB 250Xi spectrometer (Thermo Fisher Scientific Ltd - UK), equipped with a six channeltrons detection system, a monochromatic Al Kα X-ray source (hυ = 1486.7 eV) for XPS and a He lamp (He I- hν = 21.2 eV) for UPS. The spectra were acquired operating at constant pass energy of 50 eV (XPS) and 5 eV (UPS), respectively. The data were collected and processed by using the Avantage v.5.9 software (Thermo Fisher Scientific Ltd - UK).

TOF-SIMS measurements were performed with a TOF.SIMS5 (ION-TOF GmbH, Münster, Germany) secondary ion mass spectrometer, equipped with bismuth liquid metal ion gun and caesium ion sputter gun. Surface analysis data was obtained in a high lateral resolution mode using Bi+ ions (30 keV) with a pulse width of 18.4 ns and a current emission of 1.5 pA. Depth profiling measurements were performed in dual beam mode with Bi+ as the primary ion gun and Cs+ (1 keV, 40 nA current) as the sputtering beam.

The photocathodes' electron emission properties were measured by illuminating them with a simulator of concentrated sunlight. The cathodes were placed in a vacuum enclosure (base pressure ~ 7.5×10^{-8} Torr) and illuminated with a high-power Xenon arc lamp (1 kW) whose power was varied with an external power supply. The cathodic temperature was measured with a K-type thermocouple placed inside the vacuum chamber. The cathodic emission current was measured at different cathodic temperatures and the I-V cathode characteristics were determined applying a variable voltage (± 40 V) to the anodic surface.

2. Scanning Electron Microscope (SEM) investigation

Figure S1 shows the plan-view (panel A) and cross-section (panel B) of the S1 sample, i.e., the thinnest diamond layer that has been deposited on the silicon substrate. The SEM images indicate that the film is continuous and approximately 40 nm thick. The diamond film thickness of the other photocathodes has been similarly determined from SEM cross-section images.

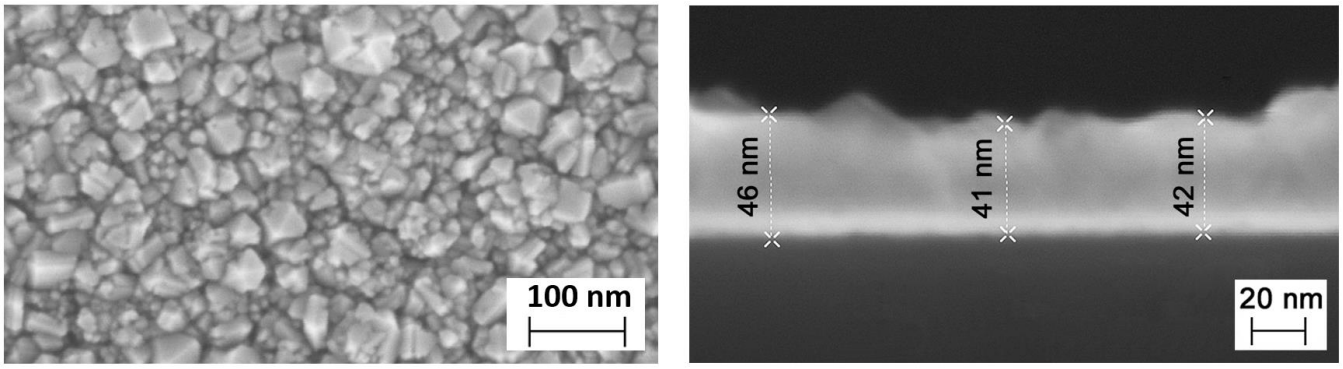

(a) (b)

Figure S1. SEM micrographs of the S1 sample: (a) plan-view, (b) cross-section.

3. Additional details on the KPFM analysis

The use of the metal clip for grounding the sample is critical, as the accumulation of electrostatic charge can significantly influence KPFM measurements, potentially perturbing the results and complicating data interpretation. So firstly, the position and the role of the metal clip has been verified and checked for obtaining a reliable comparison of the samples.

The measurements were acquired, filtered, and analysed using the AIST-NT SPM control software, which automatically sets the ideal measurement conditions. The microscopies were performed using a silicon pyramidal tip (MikroMasch HQ:NSC14/Al BS; Wetzlar, Germany) with a characteristic radius of ~8 nm, which was rendered conductive through a gentle contact with a substrate. Subsequently, the measurements were calibrated starting with the calculation of the tip's work function, following the procedure proposed by Pablo A. Fernández Garrillo et al. [**C.1**]. Using this procedure, the probe's work function was estimated to be about 4.7 eV.

Moreover, to estimate the experimental reproducibility of V_{CPD} values, a microscopy image was performed more times on the same area under identical conditions, discovering that there was about 5% margin of error. The observed area for each sample corresponded to 2 µm x 2 µm with a resolution of 500 pixels x 500 pixels, yielding a lateral resolution of 10 nm. The acquisition rate was set at 0.7 Hz with 60 nm of tapping mode amplitude.

Through the AIST program it was possible to determine the histogram of the V_{CPD} values obtained for each sample. The histogram is made up of 250000 V_{CPD} values, corresponding to the 250000 pixels used for each image, with the columns divided into 100 value ranges. The AFM and KPFM microscopies are reported in the paper, whereas the histograms and V_{CPD} values at which each histograms reaches its maximum are presented in Figure S2.

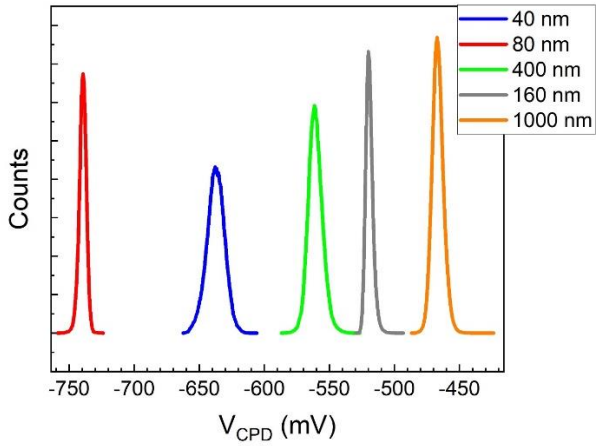

(a)

Film thickness (nm)	*V_{CPD} Peak max (mV)*
40	-636.6
80	-738.8
180	-520.3
550	-560.9
1040	-466.9

(b)

Figure S2. Histograms (a) and table of V_{CPD} values at which each histograms reaches its maximum (b).

Furthermore, through these histograms, it was possible to estimate the weighted work function ϕ^* using the following relations [1-3]:

$$\phi^* = \phi_{tip} + eV_{CPD}^*$$

$$\text{with } V_{CPD}^* = \sum_{i=1}^{100} \frac{VCPD_i \, x \, pixel_i}{pixel_i}$$

$$\text{And } \sum_{i=1}^{100} pixel_i = 250000$$

Through a graphical analysis of the KPFM images, it has been also possible to estimate the area occupied by grain boundaries relative to the total area of the polycrystalline films. In particular, grayscale images were transformed into binary images (see Figure S3). This transformation allowed discriminating the grain boundaries of the nanocrystals by applying the same level of filtering in the formation of such images.

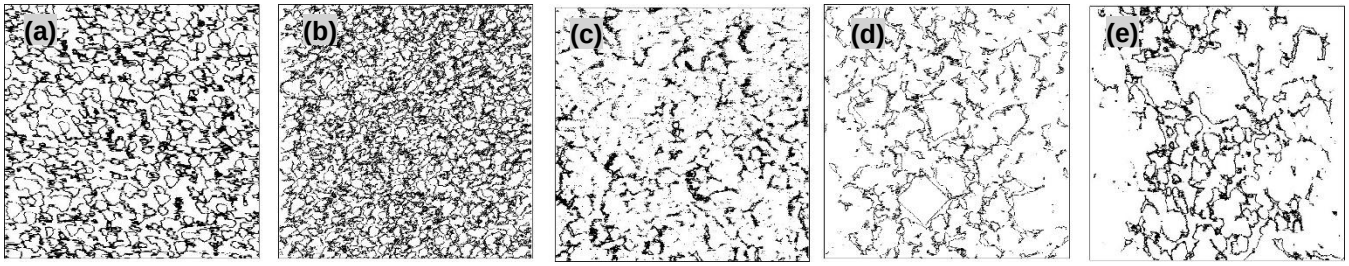

Figure S3. Binary images of KPFM analysis of 40 nm (a), 80 nm (b), 180 nm (c), 500 nm(d) and 1040 nm (e)diamond film thickness.

In this way, the grain boundary to total area ratios (A_{GB}/Atot) were estimated by the ratio between the sum of pixels switched on and the total number of pixels corresponding to 250000 pixels per image. All the obtained values of this ratio are summarized in Table S1. As shown from the analysis of the Raman spectroscopy data, the trend of the area ratio values as a function of film thickness shows a minimum for the sample S2 with thickness of 80 nm (see Figure S4, where also the value of the work function has been plotted).

Table S1. Estimated AGB/Atot and *Φ.**

Film thickness (nm)	A_{GB}/Atot	*Φ* (eV)*
40	0.25	4.06
80	0.30	3.96
180	0.14	4.18
550	0.11	4.14
1040	0.12	4.25

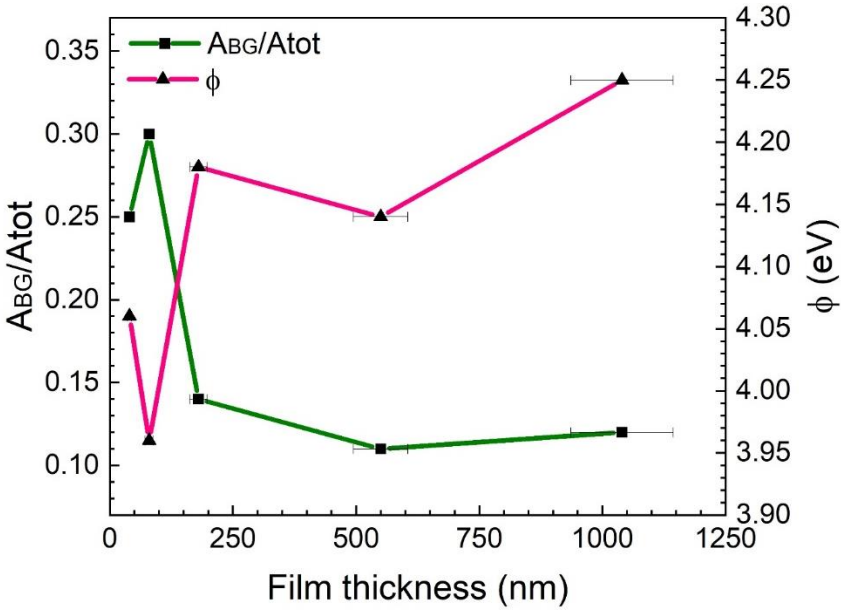

Figure S4. ABG/Atot and Φ as a function of the diamond film thickness.

[C.1] Pablo A. Fernández Garrillo, Benjamin Grévin, Nicolas Chevalier, Łukasz Borowik; Calibrated work function mapping by Kelvin probe force microscopy. *Rev. Sci. Instrum.* 1 April 2018; 89 (4): 043702. DOI: 10.1063/1.5007619.

4. Time-of-Flight Secondary Ion Mass Spectroscopy (TOF-SIMS) data

Figure S5 shows the results coming from TOF-SIMS depth profiling experiments for the S1 (40 nm) and S2 (80 nm) samples deposited on heavily B-doped silicon substrate. The behavior of ion signal intensity values for C, Si and B as a function of the sputtering time is reported. It is evident that the boron ion signal has no counts throughout the entire nanocrystalline diamond film thickness for both samples. On the contrary, as expected, the boron was detected in the silicon substrate. A slight diffusion of boron atoms from silicon substrate to the NCD layer can be appreciated in both samples. The migration of boron atoms towards the surface is due to the smaller dimensions of the B atomic radius with respect to the C atoms, thus inducing a non-negligible concentration of B atoms onto the surface. Interestingly, the analysis indicates the formation of a silicon-carbon interdiffusion layer whose thickness is approximately 10-15 nm. This is consistent with the formation of SiC at the silicon-diamond interface, in agreement with literature data [**C.2**].

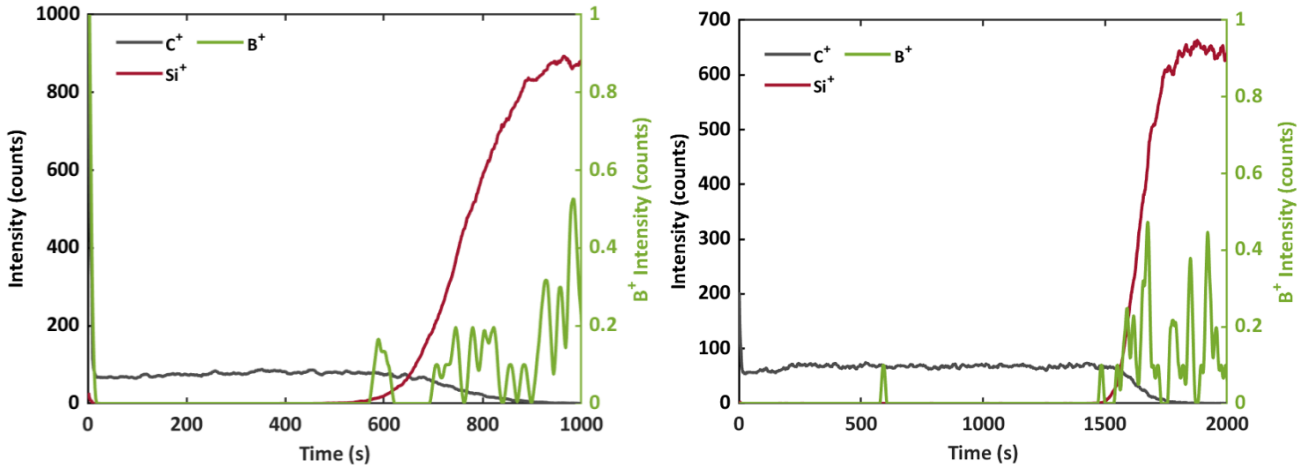

Figure S5. Depth profiling analysis of the (a) 40 nm and (b) 80 nm thick diamond photocathodes.

[C.2] Yun, J.; Dandy, D. S. A Kinetic Model of Diamond Nucleation and Silicon Carbide Interlayer Formation during Chemical Vapor Deposition. *Diamond and Related Materials* **2005**, *14* (8), 1377–1388. DOI: 10.1016/j.diamond.2005.02.008.

5. X-ray Photo-electron Spectroscopy (XPS) data and additional details on the UPS analysis

XPS measurements have been carried out on the diamond thin film (40 nm), before and after the treatment at the temperature of ~ 380 °C.
As you can see from Table S2, the C 1s spectra of every sample were fitted with 4 synthetic peaks: C 1s -1 at BE = 282.8 eV (due to the formation of carbides); C 1s -2 at BE = 284.8 eV (corresponding to sp^2/sp^3 bondings and hydrogenated carbon) and C 1s -3 at BE = 287.7 eV (C – O, C = O bonds).

From the investigation of C1s peak is not possible to assert the large presence of C-H on the surface, because its value overlaps with that of C-C and C=C. However, limiting the discussion on the comparison of the spectra before and after the PETE characterization (Fig. S6), it is possible to observe that the surface is preserved and no significant variations in the chemical composition are identified, thus suggesting that also the C-H termination is maintained.

Table S2. Quantitative results of XPS analyses (at.%) of the diamond thin films before and after the characterization at ~380 °C.

Peak	*BE (eV)*	*Atomic % Before solar furnace*	*Atomic % After heat treatment*	*Assignment*
C1s – 1	*282.8*	*1.5*	*2.0*	*Carbides*
C1s – 2	*284.8*	*90.2*	*88.9*	*C-C, C=C, C-H*
C1s - 3	*287.7*	*2.6*	*2.5*	*C–O, C=O*
O1s - 1	*532.8*	*4.9*	*3.9*	*C–O, C=O*
O1s - 2	*534.4*	*0.8*	*2.7*	*Adsorbed Oxygen*

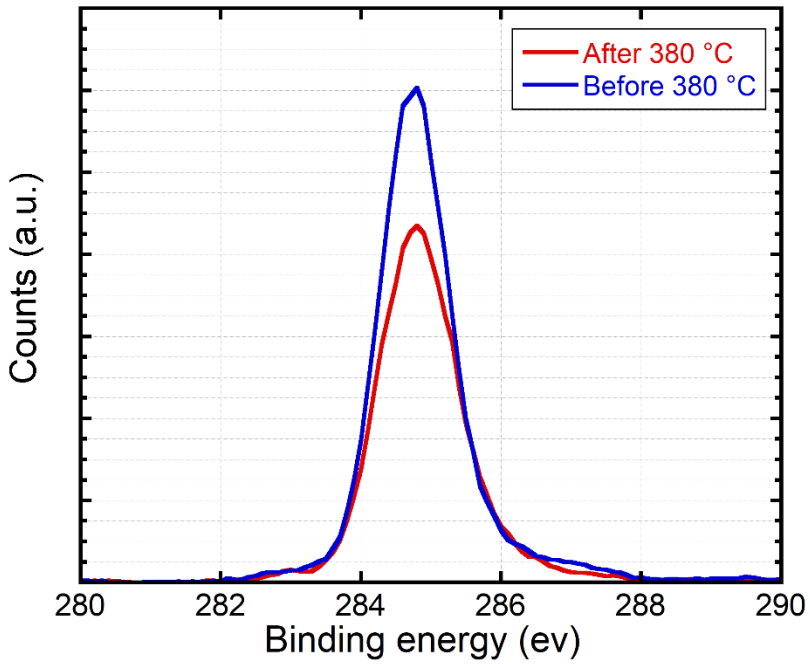

Figure S6. Peak of C1s signal of diamond thin film before and after the heat treatment at ~380 °C.

To remove the contribution of the spectrometer work function, the UPS spectra were registered applying different bias voltages to the samples (as shown in Fig. S7a as an example), following the method reported below and described elsewhere [**C.3**].

The work function (ϕ) can be calculated from the following formula after the measurement of the cut-off energy:

$$\phi = h\upsilon\ (HeI) - BE_{cut\text{-}off}$$

In principle, this method for the work function calculation cannot be applied when the material work function value is lower than the one of the spectrometer. When it happens, the sample is typically biased: the best practice is to apply different bias voltages (V) and to plot the graph of $E_{cut\text{-}off}$ vs $V^{1/2}$. Extrapolating the cut-off value to V = 0, it is possible to determine the real value of the work function. As it is shown in Fig. S7b, the application of bias voltage permits to override the spectrometer work function and to measure the real cut-off energy.

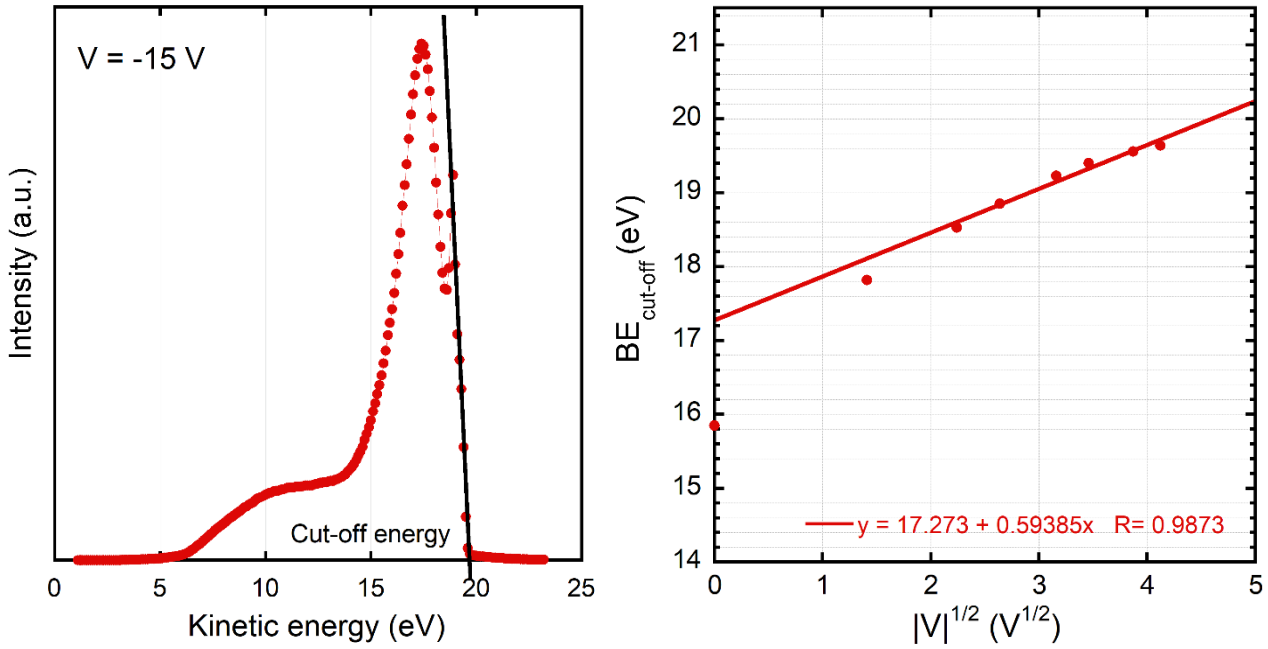

Figure S7. (a) Valence band spectrum acquired applying a bias voltage of -15 eV; (b) plot of BE_{cutoff} vs. $|V|^{1/2}$.

[C.3] Martinez, E.; Guedj, C.; Mariolle, D.; Licitra, C.; Renault, O.; Bertin, F.; Chabli, A.; Imbert, G.; Delsol, R. Electronic and chemical properties of the TaN/a-SiOC:H stack studied by photoelectron spectroscopy for advanced interconnects. *J. Appl. Phys.* **2008**, *104*, 073708. DOI: 10.1063/1.2988139.

6. Experimental setup for the PETE measurements

For PETE measurements, the solar simulator is a custom-made design equipped with a high-power Xenon arc lamp (1 kW) whose radiant power is redirected by an ellipsoidal reflector and whose electric power is finely tuned by a controllable power supply. The equipment, designed by the Paul Scherrer Institute (PSI) [**C.4**] and later acquired and installed by the DiaTHEMA group of ISM-CNR in their own laboratory, can deliver an intense radiation (achieving up to 5000 suns on a small spot of 6 mm diameter) that simulate the heat transfer characteristics of highly concentrating solar systems. The reflector is composed by three different aluminum elements with diamond machined inner surfaces. Due to its high reflectivity and its high thermal conductivity, aluminum was chosen as material for the reflector. A motorized stage allows the vertical translation of the vacuum enclosure to place the device under test precisely on the focal point. The incident flux was preliminarily evaluated using a Vatell Thermogauge 1000 water-cooled heat flux sensor. Since the electric power provided to the lamp can be finely tuned by an external power supply, the incident flux was measured at different supplied powers to obtain the exact level of irradiance.

PETE measurements were performed in an ultra-high vacuum chamber (base pressure for the measurements $\sim 7.5 \times 10^{-8}$ Torr). The temperature was measured with a K-type thermocouple placed on boron nitride (BN) shield (to avoid electrical contact with the cathode) into the lateral side of the sample holder and, in parallel, optically by the FLIR E95 IR thermal camera (using a ZnSe window for monitoring). A preliminary calibration was performed with two different K-type thermocouples, one placed in the BN within the cathode holder and another one directly put onto a reference Si cathode. Under these conditions the thermionic characterization was not performed because the cathode was electrically connected to the thermocouple but represented the case reference for the calibration considering the optical measurements. The ultimate calibration of the temperature measurement systems between K-type thermocouple and thermal camera was performed for a proper evaluation of the cathode temperature, to take into account and correct the systematic errors of the measurement methods. Electrons emitted by the sample were collected by a cooled molybdenum anode, separated from the sample by an adjustable distance. The inter-electrode distance was fixed to 50 ± 5 μm by moving the cathode holder towards the anode through a stepper motor (resolution of 0.1 μm) and an incremental optical encoder system. The translational system was previously calibrated without the presence of the two electrodes. Cathodes and anode were biased at a variable voltage to obtain current–voltage (I–V) characteristics by an electrometer (Keithley 2440) used as both voltage source and ammeter.

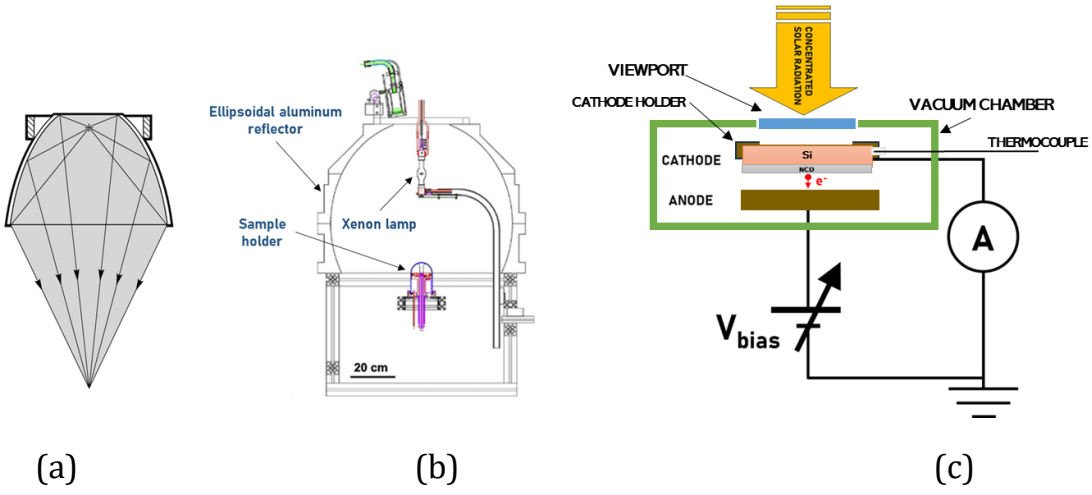

Figure S8. (a) Working principle of an ellipsoidal reflector. (b) 2D-schematic presentation of the solar simulator used in this work. (c) Scheme of the measurement setup for I-V characteristics.

[C.4] C. Guesdon et al., "PSI's 1kW imaging furnace—A tool for high-temperature chemical reactivity studies," Sol. Energy, vol. 80, no. 10, pp. 1344–1348, 2006, doi: https://doi.org/10.1016/j.solener.2005.04.028.